

# MONTE-CARLO/MOMENTS MICRO-MACRO PARAREAL METHOD FOR UNIMODAL AND BIMODAL SCALAR MCKEAN-VLASOV SDES \*

IGNACE BOSSUYT<sup>†</sup>, STEFAN VANDEWALLE<sup>†</sup>, AND GIOVANNI SAMAËY<sup>†</sup>

*Abstract.* We propose a micro-macro parallel-in-time Parareal method for scalar McKean-Vlasov stochastic differential equations (SDEs). In the algorithm, the fine Parareal propagator is a Monte Carlo simulation of an ensemble of particles, while an approximate ordinary differential equation (ODE) description of the mean and the variance of the particle distribution is used as a coarse Parareal propagator to achieve speedup. We analyse the convergence behaviour of our method for a linear problem and provide numerical experiments indicating the parallel weak scaling of the algorithm on a set of examples. We show that convergence typically takes place in a low number of iterations, depending on the quality of the ODE predictor. For bimodal SDEs, we avoid quality deterioration of the coarse predictor (compared to unimodal SDEs) through the usage of multiple ODEs, each describing the mean and variance of the particle distribution in locally unimodal regions of the phase space. The benefit of the proposed algorithm can be viewed through two lenses: (i) through the parallel-in-time lens, speedup is obtained through the use of a very cheap coarse integrator (an ODE moment model), and (ii) through the moment models lens, accuracy is iteratively gained through the use of parallel machinery as a corrector. In contrast to the isolated use of a moment model, the proposed method (iteratively) converges to the true distribution generated by the SDE.

**Key words.** Parallel-in-time; Parareal; McKean-Vlasov SDE; micro-macro; moment model; reduced model; multimodal distribution; model error

**MSC codes.** 65C30, 68Q10, 65C35, 60H35

**1. Introduction and motivation.** In this paper, we introduce an algorithm for the numerical simulation of the solution of McKean-Vlasov (mean-field) stochastic differential equations (SDEs). These equations model the dynamics over time  $t$  of an ensemble of  $P$  coupled particles  $\{X^{(p)}(t)\}_{p=1}^P$ . The evolution of an individual particle  $X^{(p)} \in \mathbb{R}^d$  can be modeled as follows:

$$(1.1) \quad \begin{aligned} dX^{(p)} &= a \left( X^{(p)}, \lambda_P \left( \{X^{(p)}\}_{p=1}^P \right), t \right) dt + b \left( X^{(p)}, \lambda_P \left( \{X^{(p)}\}_{p=1}^P \right), t \right) dW, \\ \{X^{(p)}(0)\}_{p=1}^P &\sim p_0(x) \end{aligned}$$

in which the coefficient  $a \in \mathbb{R}^d$  is the drift,  $b \in \mathbb{R}^{d \times n}$  is a diffusion coefficient,  $W \in \mathbb{R}^n$  is an  $n$ -dimensional Brownian motion. With  $\lambda_P$  we denote the empirical measure of the particle ensemble  $\{X^{(p)}\}_{p=1}^P$ , namely  $\lambda_P(x) = 1/P \sum_{p=1}^P \delta(x - X^{(p)})$  where  $\delta$  is the Dirac measure (taken from [18]). The initial distribution of the particles is denoted by  $p_0(x)$  where  $x \in \mathbb{R}^d$ . The dependence of the coefficients  $a$  and  $b$  on the empirical measure  $\lambda_P$  creates a coupling between the particles. The drift and diffusion coefficients of each particle are not only determined by the position of the

\*Submitted to the editors on DATE.

**Funding:** This project has received funding from the European High-Performance Computing Joint Undertaking (JU) under grant agreement No. 955701. The JU receives support from the European Union's Horizon 2020 research and innovation programme and Belgium, France, Germany, and Switzerland.

<sup>†</sup>Department of Computer Science, KU Leuven, Celestijnenlaan 200A, 3001 Leuven, Belgium (ignace.bossuyt1@kuleuven.be, stefan.vandewalle@kuleuven.be, giovanni.samaey@kuleuven.be)

particle itself, but also by the distribution of all the particles (see, e.g., [38] for an introduction to McKean-Vlasov SDEs). In this paper we adopt the Itô interpretation of (1.1).

In this work, we will focus on the scalar case  $d = 1$  and  $n = 1$ . In low dimensions, a histogram of the particles can be computed and visually inspected. In higher dimensions, one is typically interested in a few moments and quantities of interest (QoIs), such as the expected value of a function  $\Phi$  of the individual particles  $X^{(p)}$ , namely  $\mathbb{E}[\Phi(\{X^{(p)}\}_{p=1}^P)]$ .

Particle systems of the form (1.1) have been used to model, for instance, networks of neurons [3, 8], the synchronisation of nonlinear oscillators [23], and for the stochastic simulation of the (deterministic) Burgers equation [9]. McKean-Vlasov SDEs also arise in data assimilation methods such as ensemble Kalman filtering and other interacting particle ensemble methods for data assimilation (see for instance [12]). We will illustrate our method using examples taken from [21].

The Monte Carlo simulation of SDEs can be computationally expensive. Moment ODEs have been presented in [20, p. 139] as a cheap alternative for SDEs without mean-field coupling. They have been used, for instance, to model the stochastic spiking of neural networks in [34]. The solution to these ODEs requires no sampling, and therefore is much cheaper than a stochastic particle simulation. However, they come at the cost of a model error. As an example, the solution to moment ODEs may be nonphysical if the distribution function  $p(x)$  is not concentrated and symmetric around its mean point [34], see also [36]. SDEs with bimodal (and, more generally, multimodal) particle distributions are especially challenging.

The simulation of SDEs without mean-field interaction can easily be parallelised over all stochastic realisations. Simulations with mean-field coupling, however, are less trivially parallelisable. In [18, Figure 5], it is pointed out that there can be still a large amount of work in multilevel Monte Carlo (MLMC) and multi-index Monte Carlo schemes for McKean-Vlasov SDEs that can not be parallelised. To increase parallelism in the simulation of interacting particles, parallel-in-time methods can be envisaged. In parallel-in-time methods, the time domain is divided in different slices, on which simulation can be performed in parallel. For a history of time-parallel methods, see, e.g., [16] and [31]. For deterministic models, various methods have been proposed, including the Parareal algorithm [26], MGRIT [15] and PFASST [13]. The Parareal algorithm uses an expensive accurate time propagator, which is applied in parallel over all time slices, to correct the result of a coarse but approximate simulation method, which is applied sequentially over the time domain. The Parareal algorithm was analysed for linear ODEs and PDEs in [17].

The micro-macro Parareal algorithm [25] is a generalisation of the original Parareal algorithm, that allows to use a coarse propagator  $\mathcal{C}$  that acts on a reduced state variable. The method has been designed for multiscale (stiff) systems, where the coarse model is a cheaper non-stiff reduced model, which results in a model error in the coarse propagator. In [24], the micro-macro Parareal algorithm is applied to SDEs with scale separation, where the coarse propagator is a finite volume discretisation and the fine propagator is a Monte Carlo simulation. In [11], a similar hybrid Parareal method is proposed that couples a Monte Carlo simulation on the fine level with a Galerkin scheme on the coarse level. In [30, 29, 40], the MLMC method is combined with Parareal. The idea in those papers is to wrap a MLMC loop around a space-time multigrid solver for non-interacting particle systems. In [6] the moments of a linear SDE were used to analyse the convergence of micro-macro Parareal applied to a linear scale-separated SDE. In [14], a Parareal method has been developed where the coarse solver is a reaction rate equation (ODE), and the fine scale solver is a stochastic simulation.

In the current paper, we propose a new micro-macro Parareal variant that uses a low-dimensional moment model ODE as a coarse model, combined with a Monte Carlo discretisation

of the interacting particle system, using the Euler-Maruyama method. The key advantage is that the coarse model is very cheap to simulate.

The remainder of the paper is organised as follows. In [section 2](#), we give a brief overview of Monte Carlo methods for SDEs, which we use as a fine integrator in the Parareal method. In [section 3](#), we outline the moment ODEs that are used as a coarse Parareal integrator. It (approximatively) models the mean and variance of the particle ensemble in each disjoint region of the phase space where the SDE locally behaves unimodally. Then, in [section 4](#), we introduce the proposed MC-moments Parareal algorithm, using the moment models from [section 3](#). The algorithm is analysed on a very simple linear equation in [section 5](#). We present numerical experiments in [section 6](#) for unimodal and bimodal scalar McKean-Vlasov SDEs. [Section 7](#) presents a conclusion and proposes some future research directions.

**2. Monte Carlo simulation of SDEs.** In this subsection, we review some methods for the simulation of SDEs and introduce some notation that will be used in this paper.

*Euler-Maruyama time-stepping method for SDEs.* The most basic numerical discretisation scheme for SDEs is the Euler-Maruyama (EM) scheme (see e.g., [\[22\]](#)). For the McKean-Vlasov SDE [\(1.1\)](#), the method can be written as follows, using a timestep  $\Delta t$ , and where the index  $n$  refers to the solution at time  $n\Delta t$ :

$$(2.1) \quad X_{n+1}^{(p)} = a(X_n^{(p)}, \lambda_P(X_n), t_n)\Delta t + b(X_n^{(p)}, \lambda_P(X_n), t_n)\sqrt{\Delta t}\xi,$$

where  $\xi \in \mathbb{R}^d$  is a standard normally distributed variable,  $\xi \sim \mathcal{N}(0, 1)$ . Here and in the sequel, we write  $X_n$  instead of  $\{X_n^{(p)}\}_{p=1}^P$  in order to make notation lighter. Alternative (deterministic) methods have been developed for time simulation of McKean-Vlasov SDEs, such as the deterministic Gauss-quadrature method in [\[21\]](#).

*Weak and strong error.* When simulating SDEs, one can consider either weak or strong convergence (see e.g., [\[22\]](#)). The strong error  $E_n$  at time  $t_n$  concerns the average error on single realisations of the stochastic process:

$$(2.2) \quad E_n = \mathbb{E}[|X_n - X(t_n)|],$$

where  $X_n$  is a path obtained through numerical simulation, and  $X(t_n)$  is its exact solution. The weak error, on the other hand, considers the error on averaged quantities of the stochastic realisations, for some QoI  $\Phi(X(t))$ :

$$(2.3) \quad e_{\Phi, n} = |\mathbb{E}[\Phi(X_n)] - \mathbb{E}[\Phi(X(t_n))]|.$$

For classical SDEs under appropriate conditions, the EM method has strong order of convergence  $1/2$ , while it converges weakly with a rate of  $1$  [\[22, Theorem 14.1.5 and Theorem 10.2.2\]](#).

*Monte Carlo sampling methods.* In Monte Carlo (MC) sampling methods, the expectation of a stochastic quantity  $\mathbb{E}[\Phi(X)]$  is estimated through computing sample averages of realisations  $X^{(p)}(t)$  of the underlying SDE:

$$(2.4) \quad M_P(t) = \sum_{p=1}^P \Phi(X^{(p)}(t)),$$

where  $P$  is the number of realisations used for computing the estimate  $M_P$ .

*Monte Carlo sampling of Euler-Maruyama discretisations.* For a Monte Carlo method using  $P$  realisations wrapped around an Euler-Maruyama discrete time-stepper, the resulting estimator of  $\mathbb{E}[\Phi(X(t_n))]$  at time  $t_n = n\Delta t$  equals  $M_{P,n} = \frac{1}{P} \sum_{p=1}^P \Phi(X_n^{(p)})$  where each particle  $X_n^{(p)}$  is simulated according to (2.1).

The error on the Monte Carlo estimator  $M_{P,n}$  can be split into a bias component  $E_1$  (the time-stepping error that would arise with an infinite number of samples), and a statistical error  $E_2$  (arising from the effects of using only a finite number of samples). More precisely,

$$(2.5) \quad |M_{P,n} - M_\infty(t_n)| \leq E_1 + E_2$$

with  $E_1 = |M_{P,n} - M_P(t_n)|$  and  $E_2 = |M_P(t_n) - M_\infty(t_n)|$ . To obtain the minimal error for a given amount of computational work, the number of samples  $P$  and the number of time-steps  $N$  should be chosen so that  $P = \mathcal{O}(N^2)$ , see [19, Exercise 8.3].

**3. Moment ODEs for scalar McKean-Vlasov SDEs.** In this section, we discuss the construction and application of moment models that approximate the dynamics of McKean-Vlasov SDEs. Moment models come at a reduced computational cost as compared to stochastic particle simulations, but at the expense of a model error. However, we are not interested in the moment model on its own, but in applying the moment ODE as a coarse Parareal solver. Therefore even quite inaccurate moment models are not a priori unusable.

There exist various strategies for deriving moment models as reduced models for SDEs, see e.g., [37]. In [42], a moment model has been developed for McKean-Vlasov SDEs based on cumulants of the particle distribution. In this text, we generalize a technique from [34] which was proposed to approximate classical SDEs.

*Background: moment equation for SDEs without mean-field coupling.* For scalar classical SDEs (1.1) with  $a(X^{(p)}, \lambda_P, t) = a(X^{(p)}, t)$  and  $b(X^{(p)}, \lambda_P, t) = b(X^{(p)}, t)$ , an approximate moment ODE for the mean  $M \approx \mathbb{E}[\{X^{(p)}\}_{p=1}^P]$  and variance  $\Sigma \approx \mathbb{V}[\{X^{(p)}\}_{p=1}^P]$  reads (see [34]):

$$(3.1) \quad \begin{aligned} \frac{dM}{dt} &= a(M, t) + \frac{1}{2} b_{XX}(M, t) \\ \frac{d\Sigma}{dt} &= [2a_X(M, t) + b_X(M, t)^2] \Sigma + b(M, t)^2, \end{aligned}$$

where  $a_X$  and  $b_X$  denote the derivatives of  $a$  and  $b$  with respect to their first argument, and  $b_{XX}$  denotes the second derivative of  $b$  with respect to its first argument  $X$ . The moment description works well if the distribution function  $p(x)$  is concentrated and symmetric around its mean [34].

*Section overview.* In the section below we propose two generalisations: (i) we generalize this moment model to McKean-Vlasov SDEs (see subsection 3.1) and (ii) we propose a technique that is also applicable to bimodal SDEs, a situation where the distribution is typically not concentrated around its mean point (see subsection 3.2). The proposed moment models are exact for linear McKean-Vlasov SDEs (see Lemma 3.1), but approximative for nonlinear systems.

**3.1. Moment ODEs for McKean-Vlasov SDEs with unimodal distributions.** We first consider a special case of the McKean-Vlasov SDEs (1.1), namely SDEs where the mean-field effect only goes via the mean of a function  $f$  of the particles:

$$(3.2) \quad dX^{(p)} = a(X^{(p)}, \mathbb{E}[f(X^{(p)})], t)dt + b(X^{(p)}, \mathbb{E}[f(X^{(p)})], t)dW.$$

As a generalisation of the moment model (3.1), we propose an approximate moment model (ODE) for the mean  $M \approx \mathbb{E}[\{X^{(p)}\}_{p=1}^P]$  and variance  $\Sigma \approx \mathbb{V}[\{X^{(p)}\}_{p=1}^P]$  of the scalar McKean-Vlasov SDE

(3.2):

$$(3.3) \quad \begin{aligned} \frac{dM}{dt} &= a(M, f(M), t) + \frac{1}{2}b_{XX}(M, f(M), t) & M(0) &= \mathbb{E}[X(0)] \\ \frac{d\Sigma}{dt} &= [2a_X(M, f(M), t) + b_X(M, f(M), t)^2] \Sigma + b(M, f(M), t)^2, & \Sigma(0) &= \mathbb{V}[X(0)] \end{aligned}$$

where the derivatives of the drift and diffusion coefficients are taken w.r.t. their first arguments. The design of the moment model (3.3) is motivated by the following property.

LEMMA 3.1. *For the linear McKean-Vlasov SDE*

$$(3.4) \quad dX = (A(t)X + A_E(t)\mathbb{E}[X] + A_0(t)) dt + (B(t)X + B_E(t)\mathbb{E}[X] + B_0(t)) dW,$$

the moment equations (3.3) provide an exact description of the mean and variance.

*Proof.* See Appendix A. □

*Remark 1* (Enriching the moment model with higher-order Taylor series information). For SDEs with nonlinear drift functions, it can be interesting to add more terms in the moment model. Instead of  $\mathbb{E}[f(X)] \approx f(M)$ , one can write

$$(3.5) \quad \mathbb{E}[f(X)] \approx f(M) + \frac{\Sigma}{2}f''(M),$$

where  $M = \mathbb{E}[X]$ . This approximation can be obtained from the Taylor series,

$$(3.6) \quad f(X) = f(M) + (X - M)f'(M) + \frac{(X - M)^2}{2}f''(M) + \frac{(X - M)^3}{6}f'''(M) + \dots$$

and taking the expectation.

As an example, we consider the unimodal plane rotator, taken from [21] and [23]:

$$(3.7) \quad dX^{(p)} = \left[ \frac{K}{P} \sum_{q=1}^P \sin(X^{(q)} - X^{(p)}) - \sin(X^{(p)}) \right] dt + \sqrt{2k_B T} dW \quad \text{with} \quad X^{(p)}(0) \sim \mathcal{N}\left(\frac{\pi}{4}, \frac{3\pi}{4}\right),$$

where each time point every particle  $X^{(p)}$  is shifted modulo  $2\pi$  into the interval  $[0, 2\pi]$ . The corresponding first-order approximate moment model reads

$$(3.8) \quad \begin{aligned} \frac{dM}{dt} &= -\sin(M) \\ \frac{d\Sigma}{dt} &= -2(-K - \cos(M))\Sigma + \sigma^2. \end{aligned}$$

Using (3.5), a higher-order moment model can be constructed as follows:

$$(3.9) \quad \begin{aligned} \frac{dM}{dt} &= -\sin(M) + \frac{\Sigma}{2\sin(M)} \\ \frac{d\Sigma}{dt} &= -2\left(-K - \cos(M) + \frac{\Sigma}{2\cos(M)}\right)\Sigma + \sigma^2. \end{aligned}$$

We illustrate in Figure 3.1, that adding higher-order information improves the model. In the left panel of Figure 3.1, the first order approximation (3.8) is compared to the mean of a Monte Carlo Euler-Maruyama discretisation of the underlying SDE (3.7). In the right panel, the same experiment is done with the enriched moment model (3.9). Visually, it can be concluded that the Taylor enrichment leads to a more accurate moment model.

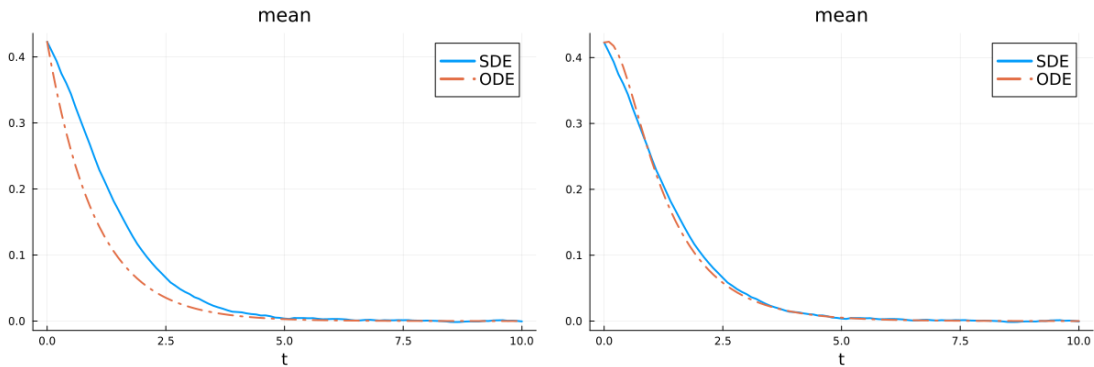


Fig. 3.1: Mean of plane rotator model: (left) first-order moment model (3.8), (right) with Taylor enrichment (3.9). For the MC simulation of the McKean-Vlasov SDE,  $10^5$  particles are used.

**3.2. Moment ODEs for McKean-Vlasov SDEs with bimodal distribution.** The solution to moment models may be nonphysical if the distribution function  $p(x)$  is not concentrated and symmetric around its mean point [34], see also [36]. Bimodal SDEs are especially challenging.

*Main idea.* The technique that we propose consists in creating a distinct moment model  $(M_i, \Sigma_i)$  for each non-overlapping region of attraction of the phase space, and coupling them. The model does not explicitly account for possible transitions to different metastable regions over time. The technique is based on intuition rather than on mathematically rigorous derivations.

*Computation of regions of attraction.* With the term *region (basin) of attraction*  $\mathcal{D}_i$ , which we here define loosely, we mean the region in which one mode of a multimodal distribution lives. The boundaries of these regions (called *separatrices*) can be computed, for instance, based on an analysis of the invariant distribution McKean-Vlasov SDE, see for instance [39] or [28]. In this paper, we assume that separatrices are known a priori, although we admit that this may be an unrealistic assumption in practice (see also future work).

*Definition and construction of moment models for classical bimodal SDEs.* We build one moment model for each local mean and variance  $(M_i, \Sigma_i)$  in each region of attraction  $\mathcal{D}_i$ . To each of the regions of attraction, we assign one additional ODE describing the fraction of particles that reside in  $\mathcal{D}_i$ .

We design the moment model in the region of attraction  $\mathcal{D}_i$ ,  $i = 1, 2$ . Let  $\mathbb{E}_{\mathcal{D}_i}$  and  $\mathbb{V}_{\mathcal{D}_i}$  denote the mean and variance of those particles residing in the region  $\mathcal{D}_i$ . We approximately describe the evolution of the mean  $M_i \approx \mathbb{E}_{\mathcal{D}_i}[\{X^{(p)}\}_{p=1}^P]$  and variance  $\Sigma_i \approx \mathbb{V}_{\mathcal{D}_i}[\{X^{(p)}\}_{p=1}^P]$  as follows:

$$(3.10) \quad \begin{aligned} \frac{dM_i}{dt} &= a(M_i, f(M_i), t) + \frac{1}{2} b_{XX}(M_i, f(M_i), t) & M_i(0) &= \mathbb{E}_{\mathcal{D}_i}[X(0)] \\ \frac{d\Sigma_i}{dt} &= [2a_X(M_i, f(M_i), t) + b_X(M_i, f(M_i), t)] \Sigma_i + b(M_i, f(M_i), t)^2 & \Sigma_i(0) &= \mathbb{V}_{\mathcal{D}_i}[X(0)] \end{aligned}$$

Another ODE is required to estimate the fraction of particles in each region of attraction. Such an ODE is, in general, nontrivial to find. For classical SDEs without McKean-Vlasov interaction, one could try to build a model on the basis of the invariant distribution. In practice, the behaviour of McKean-Vlasov SDEs can depend crucially on model parameters, as is illustrated with bifurcation

diagrams for instance in [23]. The choice of model parameters can, for instance, create and destroy multimodality. This makes the derivation of good moment models for McKean-Vlasov SDEs, as opposed to classical SDEs, more involved.

We emphasize that the construction of the ODE (3.10) can be somewhat ad-hoc. The main idea is however to have multiple ODEs for multimodal (McKean-Vlasov) SDEs. While we formulate a proposal for the construction of these ODEs, we admit that this design can possibly be further improved. The following example serves as an illustration of the technique.

*Example 3.2* (Classical SDE with underlying potential). We assume the following form of SDE

$$(3.11) \quad dX = \kappa(X)dt + b dW \quad \text{with} \quad X(0) \sim p_0(x).$$

We furthermore assume that the drift coefficient  $a$  can be derived from a potential  $V$ , namely  $\kappa(X) = dV(X)/dX$ . According to (3.10), we can use the following moment model in each region  $\mathcal{D}_i$ :

$$(3.12) \quad \begin{aligned} \frac{dM_i}{dt} &= \kappa(M_i) & M_i(0) &= \mathbb{E}_{\mathcal{D}_i}[X(0)] \\ \frac{d\Sigma_i}{dt} &= 2\kappa(M_i)\Sigma_i + b(M_i)^2 & \Sigma_i(0) &= \mathbb{V}_{\mathcal{D}_i}[X(0)] \end{aligned}$$

This linear ODE can then be used to estimate the particle fractions  $\alpha_i$ :

$$(3.13) \quad \frac{d\alpha_i}{dt} = -\frac{\sigma^2}{2|X_i - X_{i-1}|} (\alpha_i - V_i) \quad \text{with} \quad \alpha_i(0) = \sum_p \mathbb{I}(X^{(p)} \in \mathcal{D}_i) / P.$$

Here, we define  $V_i = \exp(-V(\bar{X}_i)) / \sum_i \exp(-V(\bar{X}_i))$ , and we denote the position of the peak of the mode in region  $\mathcal{D}_i$  with  $\bar{X}_i$ . The symbol  $\mathbb{I}$  denotes an indicator function, that is,  $\mathbb{I}(x)$  equals 1 if  $x$  is true and 0 otherwise.

Let us briefly motivate the construction of this moment model. For an SDE which possesses an invariant distribution, the steady-state probability  $\alpha_i$  is estimated as  $V_i$ . The speed at which the particles approach the invariant distribution is estimated as  $\sigma^2/2|X_i - X_{i-1}|$ . It is assumed to grow proportionally with higher diffusion coefficient, i.e., with more random movement of the particles, and inversely proportionally to the distance that particles need to travel in order to arrive at the nearest local peak in the neighboring region of attraction. Intuitively,  $V_i$  corresponds to the relative height of mode  $i$  in the steady-state (invariant) distribution of the SDE (since the steady state distribution of SDE (3.11) is given by  $\exp(-V(x)/2\sigma^2)/Z$  where  $Z$  is a normalisation constant, see e.g., [32, special case of Proposition 6.1]).

If the linear decay coefficient is the same in all regions  $\mathcal{D}_i$ , it can be proven that  $\sum \alpha_i(t) = 1 \forall t$  if  $\sum \alpha_i(0) = 1$ . This means that no particles are created nor disappear in the ODE (3.13).

*Example 3.3* (SDE with generalised double-well potential). We consider the SDE

$$(3.14) \quad dX^{(p)} = -\left(4\alpha(X^{(p)})^3 - 2\gamma X^{(p)} - \beta\mathbb{E}[X] + J\sqrt{\frac{a}{2b}}\right) dt + \sigma dW \quad \text{with} \quad X(0) \sim \mathcal{N}(m_0, 0.8).$$

Here,  $\alpha$ ,  $\beta$ ,  $\gamma$  and  $J$  are model parameters. Without mean-field term  $\beta\mathbb{E}[X]$ , the drift term of SDE (3.14) can be derived from the potential

$$(3.15) \quad V(X) = aX^4 - bX^2 + J\sqrt{\frac{a}{2b}}X.$$

If  $J = 0$ , the potential  $V$  is symmetric around  $X = 0$ .

We present some numerical experiments in figures [Figure 3.2](#) and [Figure 3.3](#). We choose the model parameters  $a = 1/4$ ,  $\gamma = 1/2$ ,  $\beta = 0.3$  (nonzero mean-field coupling),  $m_0 = 1.2$  (nonzero initial condition) and  $\sigma = 1$ . The remaining model parameter  $J$  is specified in the caption of the figures. We observe that the model parameters have an influence on the approximation power of the moment model, where the level of asymmetry has a large influence. Remark also that the SDE is unimodal for large values of  $\beta$ .

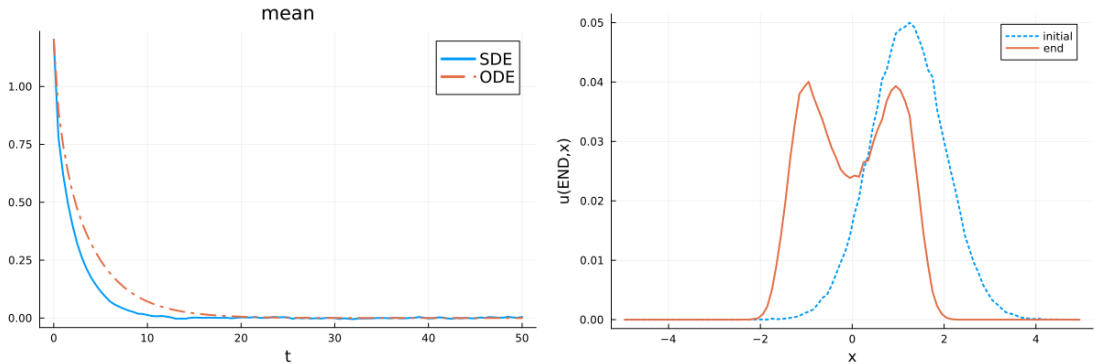


Fig. 3.2: Illustration of moment model.  $J = 0$  (symmetric potential). For the MC simulation of the McKean-Vlasov SDE,  $10^5$  particles are used.

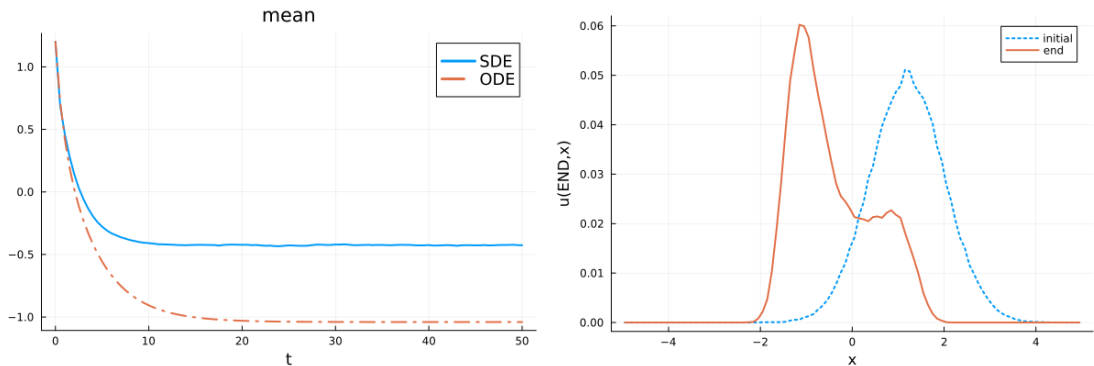


Fig. 3.3: Illustration of moment model.  $J = 0.5$  (asymmetric potential). For the MC simulation of the McKean-Vlasov SDE,  $10^5$  particles are used.

**4. The MC-moments Parareal algorithm.** In this section, we formulate the newly proposed MC-moments Parareal method.

First, we review the Parareal algorithm. Its two ingredients are (i) a fine propagator  $\mathcal{F}$ , which is accurate but computationally expensive, and (ii) a coarse propagator  $\mathcal{C}$  which is cheaper but less

accurate. Iterations of the Parareal algorithm [26] can be written as follows:

$$(4.1) \quad \begin{aligned} u_{n+1}^0 &= \mathcal{C}(u_n^0) \\ u_{n+1}^{k+1} &= \mathcal{C}(u_n^{k+1}) + \mathcal{F}(u_n^k) - \mathcal{C}(u_n^k). \end{aligned}$$

here,  $u_n^k$  is the approximation at time point  $n$  and at iteration  $k \geq 0$ . The fine propagator  $\mathcal{F}$  is used in parallel over all time slices; the coarse propagator  $\mathcal{C}$  is applied sequentially over the whole time domain in each iteration.

**4.1. Micro-macro Parareal.** In micro-macro Parareal [25], the coarse propagator acts not on the original state variable  $u$  (micro state), but on a reduced version  $\rho$  (macro state). The restriction operator  $\mathcal{R}$  extracts macro information from a micro state ( $\rho = \mathcal{R}(u)$ ). The lifting operator  $\mathcal{L}$  provides a micro state  $u$  that is consistent with a given macro state  $\rho$  ( $u = \mathcal{L}(\rho)$ ). The matching operator  $\mathcal{M}$  produces a micro state  $u$  that is consistent with a given macro state  $\rho$ , based on prior information on the micro state  $\hat{u}$  ( $u = \mathcal{M}(\rho, \hat{u})$ ).

The iterations of micro-macro Parareal are defined as follows:

$$(4.2) \quad \begin{aligned} \rho_{n+1}^0 &= \mathcal{C}(\rho_n^0) \\ u_{n+1}^0 &= \mathcal{L}(\rho_{n+1}^0), \end{aligned}$$

$$(4.3) \quad \begin{aligned} \rho_{n+1}^{k+1} &= \mathcal{C}(\rho_n^{k+1}) + \mathcal{R}(\mathcal{F}(u_n^k)) - \mathcal{C}(\rho_n^k) \\ u_{n+1}^{k+1} &= \mathcal{M}(\rho_{n+1}^{k+1}, \mathcal{F}(u_n^k)). \end{aligned}$$

If the coupling operators are chosen such that  $\mathcal{M}(\mathcal{R}u, u) = u$ , then it holds that  $\rho_n^k = \mathcal{R}u_n^k$  for all  $k$  and  $n$ . Classical Parareal [26] corresponds to the case  $\mathcal{R}(x) = x$  and  $\mathcal{L}(x, y) = \mathcal{M}(x, y) = x$ , see [25, Remark 10].

The basic idea in this paper is to use the moment model from section 3 as a coarse propagator in Parareal, while the fine propagator is a particle approximation to the SDE dynamics. Accordingly, we define coupling operators to couple these levels of description. The specific choices for  $\mathcal{R}$ ,  $\mathcal{M}$  and  $\mathcal{L}$  will be laid out in the next subsection. The fine propagator  $\mathcal{F}$  is the same for unimodal and multimodal SDEs. However,  $\mathcal{C}$ ,  $\mathcal{R}$ ,  $\mathcal{M}$  and  $\mathcal{L}$  are specific to the multimodality of the McKean-Vlasov SDE.

**4.2. Choice of coupling operators.** In the MC-moments Parareal algorithm, the micro state variable  $u_n^k$  is an ensemble of particles, denoted by  $u_n^k = [\{X^{(p)}\}_{p=1}^P]_n^k$ . Accordingly, the fine solver  $\mathcal{F}$  is a Monte Carlo discretisation of the McKean-Vlasov SDE using the Euler-Maruyama discretisation (2.1).

The coarse variable equals  $\rho_n^k = \mathcal{R}(u_n^k)$ , where the restriction operator  $\mathcal{R}$  computes the two first moments of the particle ensemble in each region of attraction  $\mathcal{D}_i$ :

$$(4.4) \quad \mathcal{R}(X) = [\mathbb{E}_{\mathcal{D}_1}[X], \mathbb{V}_{\mathcal{D}_1}[X] \dots \mathbb{E}_{\mathcal{D}_I}[X], \mathbb{V}_{\mathcal{D}_I}[X]].$$

$\mathbb{E}_{\mathcal{D}_i}$  and  $\mathbb{V}_{\mathcal{D}_i}$  denote the mean and variance of a subset of the particles residing in the region  $\mathcal{D}_i$ , and  $I$  is the total number of regions of attraction. Accordingly, the coarse solver  $\mathcal{C}$  is a unimodal ( $I = 1$ ) or multimodal ( $I > 1$ ) moment model from subsection 3.1 or subsection 3.2 respectively.

For one-dimensional McKean-Vlasov SDEs, the matching operator  $\mathcal{M}$  is given as follows. It transforms a particle ensemble  $\{X^{(p)}\}_{p=1}^P$  to another particle ensemble with desired mean  $\mu_i$  and

variance  $\sigma_i$  in each region of attraction. Define  $\rho = [\mu_1, \sigma_1, \dots, \mu_I, \sigma_I]$ , then:

$$(4.5) \quad \mathcal{M} \left( \rho, \{X_{\mathcal{D}_i}^{(p)}\}_{p=1}^{P_i} \right) = \sqrt{\frac{\sigma_i}{\mathbb{V}[\{X_{\mathcal{D}_i}^{(p)}\}_{p=1}^P]}} \left( \{X_{\mathcal{D}_i}^{(p)}\}_{p=1}^{P_i} - \mathbb{E}[\{X_{\mathcal{D}_i}^{(p)}\}_{p=1}^{P_i}] \right) + \tilde{\mu},$$

where  $\{X_{\mathcal{D}_i}^{(p)}\}_{p=1}^{P_i}$  are disjoint sub-ensembles of particles, defined by their residence region  $\mathcal{D}_i$

The lifting operator  $\mathcal{L}$  is chosen as matching with respect to the initial condition of the SDE:

$$(4.6) \quad \mathcal{L}(\rho) = \mathcal{M}(\rho, \{X^{(p)}(0)\}_{p=1}^P).$$

where  $\mathcal{M}$  implements (4.5). If the McKean-Vlasov SDE is unimodal, then  $I = 1$  suffices, and the matching operator (4.5) coincides with the transformation given in [10, Section 4.3].

*Remark 2* (Choice of discretisation parameters and termination condition). In the proposed algorithm, there exist multiple sources of approximation errors: (i) statistical error which unavoidably occurs in the stochastic, Monte Carlo, approximation method, (ii) time-discretisation error (bias) through the temporal discretisation at the particle level, and (iii) model error introduced through the moment model.

For the fine propagator  $\mathcal{F}$ , the time-discretisation error should be chosen of the same order as the statistical error. The model error arising from the moment approximation only enters the algorithm via the coarse propagator  $\mathcal{C}$ . When comparing to the exact solution of the problem, the error of the algorithm saturates on the error level of the fine propagator. Once that level is reached the iteration can stop. We do not, however, include this stopping criterion in the MC-moments Parareal algorithm.

**5. Analysis of MC-moments Parareal.** In this section we provide a short convergence analysis of the proposed algorithm, under very restrictive conditions on the type of McKean-Vlasov SDE. We additionally assume that there is no statistical error and no time-discretisation error in the coarse and fine propagators.

*Remark 3.* Although moment models for linear systems provide an exact description of the mean and variance, we see two reasons why MC simulations of linear systems are still interesting (and thus also the MC-moments Parareal algorithm for linear systems): (i) if the initial distribution is unknown, the moment model cannot capture the shape of the probability density function, and (ii) if the QoI is nonlinear, a moment model alone is in general not able to describe the time evolution of the QoI.

**5.1. Exactness property of micro-macro MC-moments Parareal.** In [25], it is proven that the algorithm satisfies the exactness property, namely  $u_n^k = u_n$  if  $k \geq n$  if the matching operator satisfies  $\mathcal{M}(\mathcal{R}u, u) = u$ ,  $\forall u \in \mathbb{R}^d$ .

LEMMA 5.1 (Exactness property of micro-macro MC-moments Parareal). *In the absence of statistical error, the MC-moments Parareal iterations satisfy the exactness property  $\mathbb{E}[\{X^{(p)}\}_{p=1}^P]^k_n = \mathbb{E}[\{X_n^{(p)}\}_{p=1}^P]$  if  $k \geq n$ .*

*Proof.* Using the definition of the matching operator (4.5), it holds that

$$(5.1) \quad \mathcal{M}(\mathcal{R}u, u) = \mathcal{M}([\mu, \sigma], X) = X.$$

Thus the exactness property holds, based on the theorem in [25], mentioned above.  $\square$

**5.2. Convergence of micro-macro Parareal on the scalar Ornstein - Uhlenbeck SDE with model error.** In this subsection, we study convergence of the MC-moments Parareal algorithm for a linear Ornstein-Uhlenbeck model with a perturbed coarse propagator. We first introduce the model problem and then we give a theoretical convergence bound. The analysis is carried out assuming the absence of statistical error.

The assumption that there is no statistical error in the fine solver allows us to adopt the convergence theory of the classical Parareal algorithm, which is more extensive than for micro-macro Parareal. The main motivation behind this analysis is to be able to gauge the influence of the model error in the coarse solver.

*Example 5.2* (Perturbed generalised Ornstein-Uhlenbeck SDE). For the fine Parareal solver  $\mathcal{F}$ , we consider the following Ornstein-Uhlenbeck SDE:

$$(5.2) \quad dX^{(p)} = (aX^{(p)} + a_E \mathbb{E}[X])dt + BdW.$$

The coarse solver  $\mathcal{C}$  consists of the ODE

$$(5.3) \quad \begin{aligned} \frac{dM}{dt} &= (a + a_E)(1 + \epsilon_M)M \\ \frac{d\Sigma}{dt} &= 2a(1 + \epsilon_M)\Sigma + B^2(1 + \epsilon_V)^2, \end{aligned}$$

where  $\epsilon_E$  and  $\epsilon_V$  are artificial perturbation parameters. As  $\epsilon_E, \epsilon_V \rightarrow 0$ , the coarse model gets closer to the fine model.

The convergence bound for classical Parareal follows directly from the analysis in [17]. A summary of the proof is given in [Appendix B.3](#).

**LEMMA 5.3** (Superlinear and linear bounds for Parareal on linear scalar ODEs). *Assume an affine coarse propagator as  $\mathcal{C}(t, u) = Gu + g(t)$ , with  $|G| < 1$ , and an affine fine propagator  $\mathcal{F}(t, u) = Fu + f(t)$ . Then, the error on the classical Parareal iterates satisfies the following error bounds. On a short time interval (superlinear bound):*

$$(5.4) \quad \max_{1 \leq n \leq N} |u(t_n) - U_n^k| \leq \frac{\rho_s^k}{k!} \prod_{j=1}^k (N - j) \max_{1 \leq n \leq N} |u(t_n) - U_n^0|.$$

*On long intervals (linear bound)*

$$(5.5) \quad \max_{1 \leq n \leq N} |u(t_n) - U_n^k| \leq \rho_l^k \max_{1 \leq n \leq N} |u(t_n) - U_n^0|,$$

where  $\rho_s = |F - G|$  and  $\rho_l = \frac{|F - G|}{1 - |G|}$ .

*Application of convergence result to model-perturbed Ornstein-Uhlenbeck process.* For the convergence of the mean and variance, the superlinear convergence factor can be bounded as follows:

$$(5.6) \quad \begin{aligned} \rho_{s,M} &\leq C_{s,M} |a\epsilon_M| \\ \rho_{s,\Sigma} &\leq C_{s,\Sigma} |2a\epsilon_M|. \end{aligned}$$

The linear convergence rates for the mean and variance can be bounded as follows:

$$(5.7) \quad \begin{aligned} \rho_{l,M} &\leq C_{l,M} \frac{|(a + a_E)\epsilon_M|}{1 - a(1 + \epsilon_M)} \\ \rho_{l,\Sigma} &\leq C_{l,\Sigma} \frac{|(2a\epsilon_M)|}{1 - a(1 + \epsilon_M)}. \end{aligned}$$

These relations clarify the relation of the convergence factors as a function of the perturbation parameters  $\epsilon_M$  and  $\epsilon_V$ . The proof can be found in [Appendix C](#). The convergence factors in (5.6) and (5.7) do not depend on  $\epsilon_V$ . Intuitively, this can be seen from lemma 5.3 by noting that the linear decay factors in (5.3) do not contain  $\epsilon_V$ . A proof is given in [Appendix C](#).

### 5.3. Cost and efficiency analysis.

*Reduction in wall-clock time.* In this analysis we assume that the simulation cost of the coarse model and of the fine model do not vary over time. Denoting these costs over one time interval  $\Delta t$  as  $T_{C,N}$  and  $T_{F,N}$ , we typically have that  $T_{F,N} \gg T_{C,N}$  but we do not further specify these costs, as these depend on the number of particles and on the parallel implementation. The cost for computing the restriction is denoted  $T_R$ , the cost for matching  $T_M$ . These costs are in general not negligible as they also depend on the number of particles and on the implementation.

We study the cost (waiting time) for a non-pipelined version. For a pipelined version of classical Parareal, see e.g., [27] and [35]. The micro-macro Parareal solution after  $k$  iterations, starting from  $k = 0$  with  $N$  subintervals takes the following wall-clock time:

$$(5.8) \quad T_N = NT_{C,N} + k(NT_{C,N} + T_{F,N} + T_R + T_M).$$

The matching and restriction can be computed in parallel over all time intervals.

The parallel speedup is equal to

$$(5.9) \quad S_N = \frac{NT_{F,N}}{T_N} = \frac{NT_{F,N}}{NT_{C,N} + k(NT_{C,N} + T_{F,N} + T_R + T_M)}.$$

For given simulation costs, the speedup  $S_N$  can be large if the number of iterations  $k$  is small.

**6. Numerical experiments.** In this section, we test our algorithm by means of numerical experiments. Some examples are taken from [21] and also appear in [4].

**6.1. Setup of experiments.** The code with numerical experiments can be found in [5] as well as in the Supplementary Materials. It is implemented in a non-parallel way. For the MC discretisation of the McKean-Vlasov SDE, we implemented our own Euler-Maruyama code. Unless otherwise mentioned, the number of particles was  $10^4$ . The moment ODEs are solved with the Tsitouras 5/4 Runge-Kutta method with an automatic stepsize controller. This corresponds to the function `Tsit5` with adaptive step size control from [33].

As a reference solution, we consider the solution obtained at the final Parareal iteration with  $K = N$ . We consider the error on three quantities: (i) mean, (ii) variance, (iii) the particle distribution. The relative errors are measured as follows:

$$(6.1) \quad \begin{aligned} E_{\text{mean},k} &= \|\mathbb{E}[\{\{X^{(p)}\}_{p=1}^P\}_n^k] - \mathbb{E}[\{\{X^{(p)}\}_{p=1}^P\}_n^K]\|_{n,2} / \|\mathbb{E}[\{\{X^{(p)}\}_{p=1}^P\}_n^K]\|_{n,2} \\ E_{\text{var},k} &= \|\mathbb{V}[\{\{X^{(p)}\}_{p=1}^P\}_n^k] - \mathbb{V}[\{\{X^{(p)}\}_{p=1}^P\}_n^K]\|_{n,2} / \|\mathbb{E}[f(\{\{X^{(p)}\}_{p=1}^P\}_n^K)]\|_{n,2} \\ E_{\mathcal{W},k} &= \|\mathcal{W}(\{\{X^{(p)}\}_{p=1}^P\}_n^k, \{\{X^{(p)}\}_{p=1}^P\}_n^K)\|_{n,2} / \|\mathbb{E}[\{\{X^{(p)}\}_{p=1}^P\}_n^K]\|_{n,2}, \end{aligned}$$

where  $\|\cdot\|_{n,2}$  denotes the 2-norm over all time indices  $n$ . With  $\mathcal{W}(\mu, \nu)$  we denote the Wasserstein distance between the probability distributions  $\mu$  and  $\nu$  [41, Definition 6.1]:

$$(6.2) \quad \mathcal{W}^{(l)}(\mu, \nu) = \inf_{\pi \in \Pi(\mu, \nu)} \left[ \int_{\mathcal{X}} d(x, y)^l d\pi(x, y) \right]^{\frac{1}{l}}.$$

Here,  $l$  is the order of the Wasserstein distance and  $\Pi(\mu, \nu)$  is the set of all probability measures on  $\Omega^2$  that have marginals  $\mu$  and  $\nu$ . In a numerical implementation, we are interested in the distance between finite ensembles of particles  $\{X^{(p)}\}_{p=1}^P$  and  $\{Y^{(q)}\}_{q=1}^Q$ , instead of the distance between probability distributions  $\mu$  and  $\nu$ . The evaluation of  $\mathcal{W}^{(l)}(\{X^{(p)}\}_{p=1}^P, \{Y^{(q)}\}_{q=1}^Q)$  is then turned into the solution of a linear programming problem. We use the Julia package `ExactOptimalTransport.jl` [43] with  $l = 1$ .

For the computational experiments, we averaged the errors over 20 realisations. We vary the number of time intervals (or processors)  $N$ , while we simultaneously and proportionally vary the time horizon of the problem. I.e., the time interval equals  $[0, T] = [0, NT_0]$ . When comparing results with different numbers of subintervals, the 2-norm errors are normalised through division by  $\sqrt{N}$ .

## 6.2. McKean-Vlasov SDES with unimodal particle distribution.

*Example 6.1* (Perturbed generalised Ornstein-Uhlenbeck SDE, continuing from [Example 5.2](#)). In this example, we apply MC-moments Parareal with the SDE (5.2) as fine model and the moment ODE (5.3) as coarse solver.

The chosen parameters are  $\alpha = -1$ ,  $\beta = -0.5$ ,  $\sigma = 1/100$  and  $u_0 = 100$ ,  $\epsilon_E = 1$  and  $\epsilon_V = 1$ . The initial condition is chosen as  $p_0(X) = \delta(X - 100)$ .

In [Figure 6.1](#), we plot the convergence of the iterates with respect to the iteration number for various time horizons. For the number of Parareal subintervals  $N = 10$ , we also plot the linear and superlinear bounds from [Lemma 5.3](#).

Observe that there is an agreement between the numerical results and the theoretical bounds. On a short time horizon, the superlinear bound is close to tight. On a longer time interval, the linear bound becomes tight. For the selected parameters, increasing the time window makes the convergence slower.

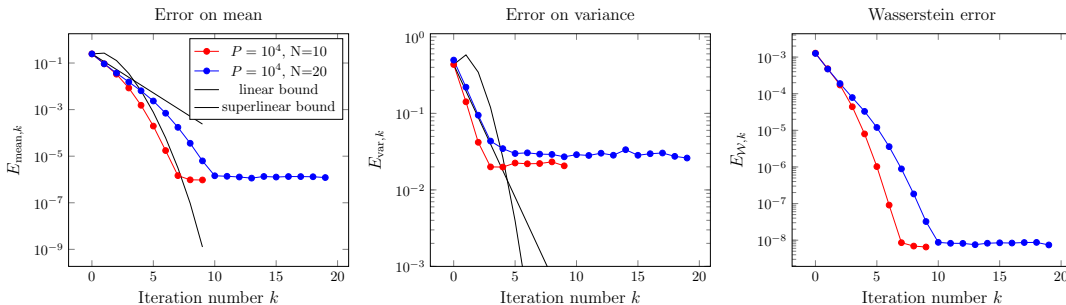


Fig. 6.1: Illustration of the MC-moments Parareal iterates: Perturbed generalised Ornstein-Uhlenbeck SDE

*Example 6.2* (Unimodal plane rotator, continuing from [Remark 1](#)). In this example we study an SDE taken from [21] and [23]. We have already studied the quality of different moment ODEs

for this SDE in remark [Remark 1](#).

(6.3)

$$dX^{(p)} = \left[ \frac{K}{P} \sum_{q=1}^P \sin(X^{(q)} - X^{(p)}) - \sin(X^{(p)}) \right] dt + \sqrt{2k_B T} dW \quad \text{with} \quad X^{(p)}(0) \sim \mathcal{N}\left(\frac{\pi}{4}, \frac{3\pi}{4}\right).$$

The moment model for the SDE (6.3) is given in [subsection 3.1](#) (see equation (3.8)).

In [21] a shift modulo  $2\pi$  is applied in each time-step. That corresponds to shifting at each timestep every particle  $X$  modulo  $2\pi$  into  $[0, 2\pi]$  in the Euler-Maruyama algorithm. This creates a unimodal distribution of the solution particles. If no such shift is applied, the SDE (3.7) possesses a multimodal particle distribution.

We choose the discretisation parameters  $[0, T] = [0, 10]$  and  $\Delta t = 1/1000$ . The coarse moment model is the Taylor-enriched ODE (3.9).

In [Figure 6.2](#) we plot the time-dependent iterates. We observe that the mean and variance converge to the true solution in just a few iterations. The same holds for the histogram of the particles (the reference solution, which corresponds to  $k = K$ , is colored in blue). In [Figure 6.3](#) we plot the convergence behavior with respect to the iteration number. The error on the mean oscillates around the statistical error. For the variance and the Wasserstein error, the statistical error is reached in a few iterations.

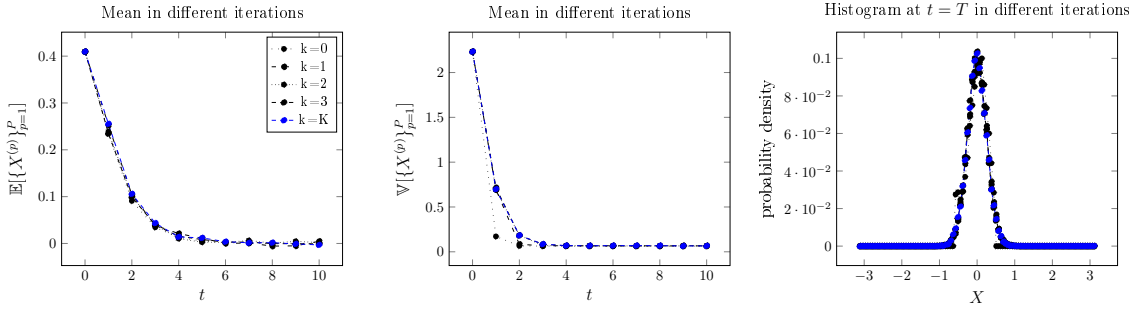


Fig. 6.2: Illustration of the MC-moments Parareal iterates: Unimodal plane rotator.

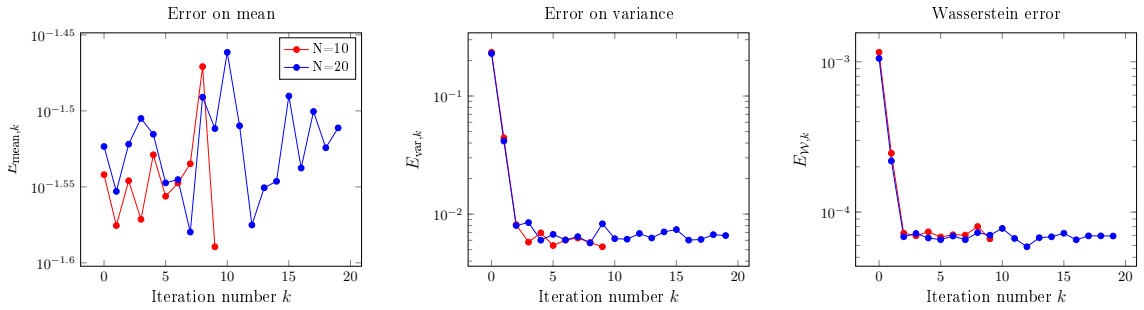


Fig. 6.3: Convergence of MC-moments Parareal: Unimodal plane rotator.

*Example 6.3* (Viscous Burgers equation). This example is taken from [9], and is also used as an example in [21]. We consider the nonlinear hyperbolic partial differential equation

$$(6.4) \quad \frac{\partial V}{\partial t} = \frac{1}{2}\sigma^2 \frac{\partial^2 V}{\partial x^2} - V \frac{\partial V}{\partial x} \quad \text{with} \quad V(0, x) = 1 - H(x).$$

The initial condition  $V(0, x)$  is a step function. If we define a particle ensemble  $\{X^{(p)}\}_{p=1}^P$  such that  $V(x) = 1 - \text{CDF}(x)$ , where CDF is the cumulative distribution function of  $\{X^{(p)}\}_{p=1}^P$ , then it is possible to associate with (6.4) the McKean-Vlasov SDE

$$(6.5) \quad dX^{(p)} = \left[ \int_{\mathbb{R}} (1 - H(X - y)) P(dy) \right] dt + \sigma dW \quad \text{with} \quad X(0) = 0$$

with all particles initialised at the origin. The McKean-Vlasov SDE (6.5) can be rewritten as follows

$$(6.6) \quad dX^{(p)} = (1 - \text{CDF}(X))dt + \sigma dW \quad \text{with} \quad X(0) = 0.$$

*Derivation of the moment model.* The SDE (6.6) violates the assumption that was used in subsection 3.1. Indeed, the drift and diffusion coefficients depend on the full distribution and not only on some quantity of interest of the particles. Here, it does not suffice to assume that the particle distribution is well concentrated around its mean point. Instead more fundamental assumptions on the distribution need to be made.

Using the assumption that the particles are normally distributed (also called a Maxwellian distribution), an approximate moment model for (6.6) reads

$$(6.7) \quad \begin{aligned} \frac{dM}{dt} &= 1 - \text{CDF}|_{(X=M)} = \frac{1}{2} \\ \frac{d\Sigma}{dt} &= -\frac{2}{\sqrt{2\pi}}\sqrt{\Sigma} + \sigma^2 \end{aligned}$$

We used the fact that the integral of a normal distribution from  $-\infty$  to its mean equals to 1/2, and the fact that

$$(6.8) \quad \left. \frac{d(1 - \text{CDF}(X))}{dX} \right|_{(X=m)} = -\text{PDF}(X = m) = -\frac{2}{\sqrt{2\pi\Sigma}}.$$

*Comparison of moment model with exact solution.* In [9], a formula is given for the probability density function  $u(x, t)$  of the particles:

$$(6.9) \quad u(t, x) = \frac{\text{erf}(-x/2\sigma^2 t)}{\text{erf}(-x/2\sigma^2 t) + \exp((t - 2x)/2\sigma^2)(2 - \text{erf}((t - x)/2\sigma^2 t))},$$

In fact, the moment model for the mean of the particle ensemble is exact, since the solution is a traveling wave with speed 1/2 [9]. It is possible that the variance is described more accurately if another assumption on the distribution is made.

*Extension.* If in (6.4) another initial condition was chosen, containing some samples  $X^{(p)} < 0$ , the particle system (1.1) does not suffice. Instead a weighted particle ensemble should be used to describe the system's behaviour in a stochastic way, see [7, Section 2.3]. Such a weighted particle simulation, however, is left for future work. We choose the parameters  $[0, T] = [0, 20]$ ,  $\sigma = \sqrt{0.2}$  and  $\Delta t = 1/10$ .

In [Figure 6.4](#) we plot the time-dependent iterates. For the mean, the only difference between the moment model and the MC simulation of the SDE arises through the effect of different time discretization methods and statistical errors, since the moment model [\(6.7\)](#) is exact for the mean. In [Figure 6.5](#) the convergence of the mean, variance and the Wasserstein error is plotted. The errors oscillate around the statistical error already after a few iterations. The difference in the convergence trajectories for  $N = 10$  and  $N = 20$  for the mean and the Wasserstein error in [Figure 6.5](#) (more specifically, they differ essentially with a scaling factor) is explained through our definition of the relative errors in [\(6.1\)](#) and the fact that we normalize the 2-norm errors for different  $N$  by division with  $\sqrt{N}$ . The qualitative convergence behavior, however, is the same for the mean and the Wasserstein error.

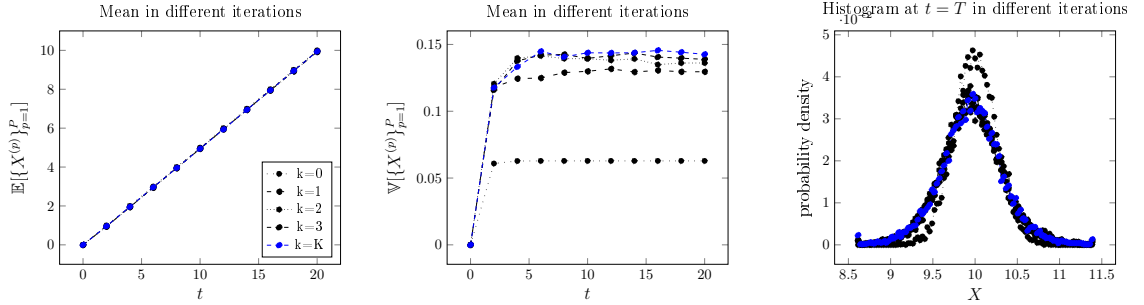


Fig. 6.4: Illustration of the MC-moments Parareal iterates: viscous Burgers equation.

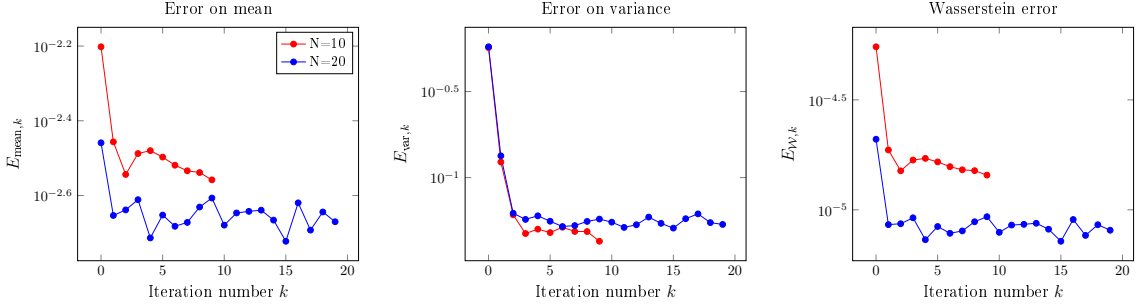


Fig. 6.5: Convergence of MC-moments Parareal: viscous Burgers equation.

### 6.3. McKean-Vlasov SDEs with bimodal particle distribution.

*Example 6.4* (McKean-Vlasov SDE with generalised bimodal potential, continuing from [Example 3.3](#)). We use the SDE with bimodal particle distribution from [Example 3.3](#), see equation [\(3.14\)](#) which is repeated here.

$$dX^{(p)} = - \left( 4\alpha \left( X^{(p)} \right)^3 - 2\gamma X^{(p)} - \beta \mathbb{E}[X] + J \sqrt{\frac{a}{2b}} \right) dt + \sigma dW \quad \text{with} \quad X(0) \sim \mathcal{N}(m_0, 0.8)$$

Recall that the parameter  $\beta$  is the strength of the particle coupling and  $m_0$  is the mean value of the initial condition of the SDE.

For the numerical experiments, we choose the model parameters  $a = 1/4$ ,  $\gamma = 1/2$ ,  $\beta = 0.3$  (nonzero mean-field coupling) and  $m_0 = 1.2$  (nonzero initial condition) and  $\sigma = 1$ . We consider two situations:  $J = 0$  (symmetric potential) and  $J = 0.5$  (asymmetric potential). Figures Figure 6.6 and Figure 6.7 show different time-dependent iterates. In both situations takes place in a few iterations. In all the considered regimes, the MC-moments Parareal algorithm rapidly converges to the statistical discretisation level. The same conclusion can be drawn from Figure 6.8 and Figure 6.9, where the error is plotted as a function of the iteration number.

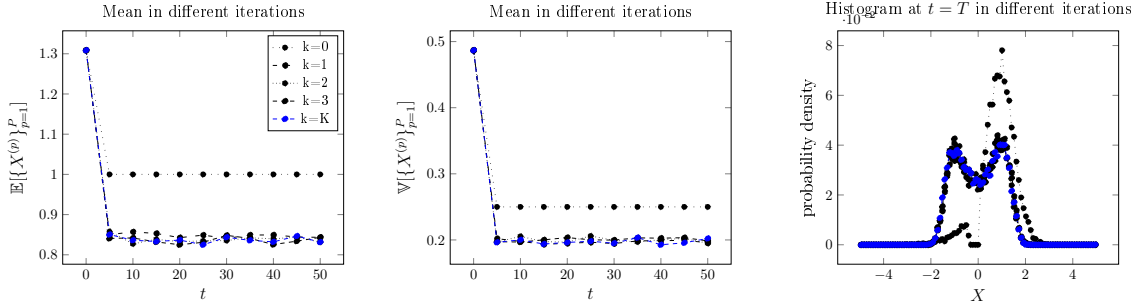


Fig. 6.6: Illustration of the MC-moments Parareal iterates: McKean-Vlasov SDE with generalised bimodal potential.  $J = 0$  (symmetric potential).

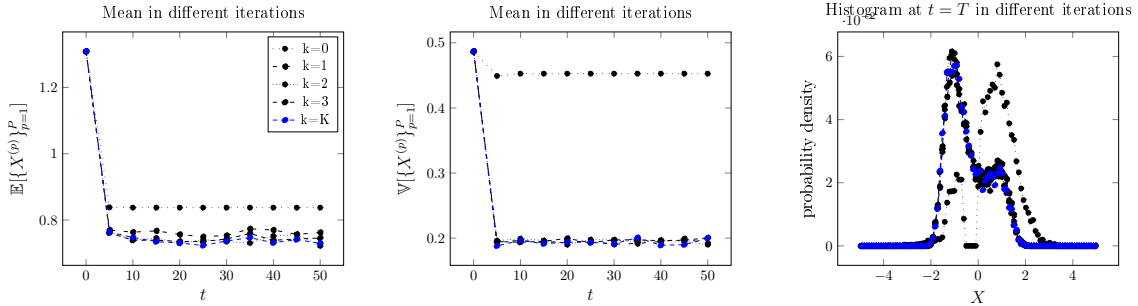


Fig. 6.7: Illustration of the MC-moments Parareal iterates: McKean-Vlasov SDE with generalised bimodal potential.  $J = 0.5$  (asymmetric potential).

**6.4. Discussion.** We numerically studied the convergence of MC-moments Parareal on a few simple scalar McKean-Vlasov SDEs by means of some numerical experiments. For our test problems, convergence takes place in a few iterations, and we observed parallel weak convergence. However, note that the observed weak scaling depends on the chosen time horizon  $T$ . If  $T$  were chosen smaller, scaling results likely would be different.

The key ingredient for the method to work for bimodal SDEs, is the introduction of several

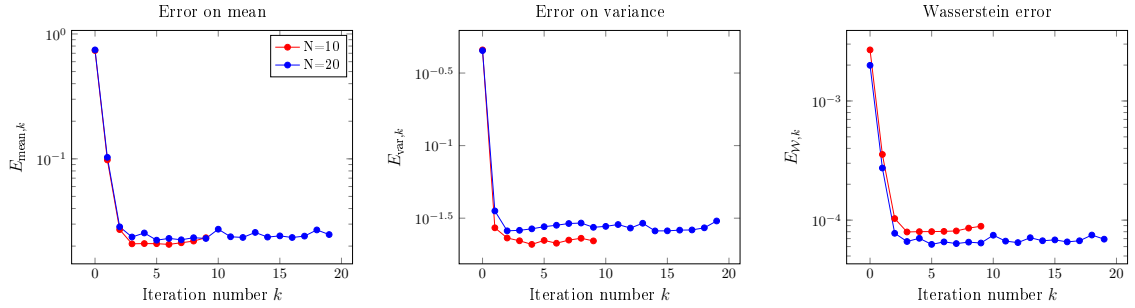


Fig. 6.8: Convergence of MC-moments Parareal: McKean-Vlasov SDE with generalised bimodal potential.  $J = 0$  (symmetric potential).

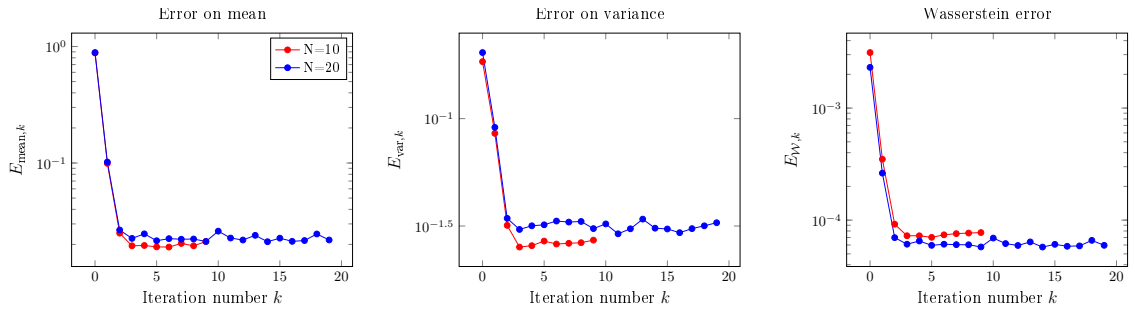


Fig. 6.9: Convergence of MC-moments Parareal: McKean-Vlasov SDE with generalised bimodal potential.  $J = 0.5$  (asymmetric potential).

moment ODEs instead of a single ODE. We also encountered SDEs for which the MC-moments Parareal method either (i) does not converge so quickly or (ii) exhibits no good parallel scaling. Examples are the polynomial drift SDE and the multimodal plane rotator from [21].

As a rule of thumb, the quality of the coarse ODE plays a crucial role for the overall convergence. It appears difficult to predict a priori, however, whether or not convergence will take place.

## 7. Conclusion and future work.

**7.1. Strengths.** The main strength of the proposed MC-moments Parareal method is that it makes use of a very cheap coarse model. That model can be derived from first principles. This may lead to a substantial gain in wall-clock time, at least in theory, if the required tolerance (i.e., statistical error of the fine solver) is not very severe.

The MC-moments Parareal algorithm also works for classical SDEs without mean-field interaction. However, on a massively parallel machine (allowing parallelisation over the then independent samples), the MC-moments Parareal algorithm would only be useful if the computation of one particle path takes longer than desired. When the number of samples is known a priori, it may be more useful to parallelise over the stochasticity rather than over time since the former could be done without a need for iterations. See also [2].

Even if a moment model on itself provides a good approximation of the SDE dynamics (mean and variance), it can still be a nontrivial task to estimate nonlinear quantities of interest. The proposed MC-moments Parareal method allows to estimate such nonlinear quantities of interest by sampling.

**7.2. Limitations.** The potential speedup with respect to sequential simulation depends very much on the approximation properties of the moment models. If the moment model gives rise to nonphysical behaviour, for instance if the variance blows up or if the variance becomes negative [36], it remains to be seen how useful the proposed technique is in practice. The method may have to be modified to deal with these issues.

For bimodal systems, the computation of the domains of attraction can be a compute-intensive process. Here, we assumed them to be known. Moreover, for McKean-Vlasov SDEs, it can already be hard to predict whether the solution is multimodal or not, depending on parameter values. If this information can be obtained from a steady-state analysis (not a time simulation), we believe that the proposed MC-moments Parareal algorithm can still be useful.

**7.3. Future work.** We finally finish with some suggestions for future research.

A next step would be to develop an adaptive variant of the MC-moments Parareal algorithm where multimodality is discovered on-the-fly, and where moment ODEs are then dynamically added or removed. We think that this could for instance be realised using clustering algorithms.

Our current Julia implementation does not contain any parallelisation. A next step would be to implement the algorithm in parallel and test it on a massively parallel machine.

**Acknowledgments.** We thank the following colleagues for discussions, suggestions, ideas and advice related to the content of this manuscript: Arne Bouillon, Tom Kaiser, Vince Maes, Ausras Pogoželskyte (at the PinT workshop 2022), and Hannes Vandecasteele.

## Appendix A. Proof of exactness of moment model for linear McKean-Vlasov SDEs.

*Proof.* The proof is based on a similar procedure as mentioned in [21] for a linear Ornstein-Uhlenbeck SDE. See also [1, Section 8.4 and 8.5]. Writing Itô's lemma for the SDE (3.2) and the test functions  $f(x) = x$  and  $f(x) = (x - M)^2$ , where  $M = \mathbb{E}[X]$ , and then taking expectations leads to the desired result, namely the moment model (3.3) with  $a(X, \mathbb{E}[X], t) = A(t)X + A_E \mathbb{E}[X] + A_0(t)$ ,  $b(X, \mathbb{E}[X], t) = B(t)X + B_E \mathbb{E}[X] + B_0(t)$ , thus  $a_X = A(t)$  and  $b_X = B(t)$  and  $b_{XX} = 0$ . We first write Itô's lemma with the test function  $f(x) = x$ :

$$(A.1) \quad dX = (A(t)X + A_E(t)\mathbb{E}[X], t + a(t)) dt + (B(t)X + B_E(t)\mathbb{E}[X] + b(t)) dW.$$

Taking expectation immediately leads to the evolution ODE for  $M$  in (3.3). For the test function  $f(x) = (x - M)^2$  we write Itô's lemma as follows:

$$(A.2) \quad d(X - M)^2 = \left[ 2(X - M) (A(t)X + A_E(t)\mathbb{E}[X] + a(t)) + (B(t)X + B_E(t)\mathbb{E}[X] + b(t))^2 \right] dt + 2(X - M) (B(t)X + B_E(t)\mathbb{E}[X] + b(t)) dW.$$

Equivalently, after rewriting (A.2) and using the fact that  $(BX + Q)^2 = B^2(X - M)^2 + Q^2 +$

$2BXQ + B^2(X - M)M + B^2MX$ , we obtain

$$(A.3) \quad \begin{aligned} d(X - M)^2 = & [2(X - M)^2A(t) + 2M(X - M)A(t) + 2(X - M)(A_E(t)\mathbb{E}[X] + A_0(t)) \\ & + B(t)^2(X - M)^2 + (B_E(t)\mathbb{E}[X] + B_0(t))^2 + 2B(t)(B_E(t)\mathbb{E}[X] + B_0(t))^2X \\ & + (X - M)B(t)^2M + B(t)^2MX] dt \\ & + 2(X - M)(B(t)X + B_E(t)\mathbb{E}[X] + b(t)) dW. \end{aligned}$$

Then, upon taking expectations of (A.3) and applying the martingale property and the fact that  $\mathbb{E}[\kappa(X - M)] = 0$ , where  $\kappa$  is a constant, the exact moment ODE for the variance  $\Sigma$  is obtained:

$$\begin{aligned} d\mathbb{E}[(X - M)^2] &= 2A(t)\Sigma + B(t)^2\Sigma + (B_E(t)M + B_0(t))^2 + 2B(t)(B_E(t)M + B_0(t))^2M + B(t)^2M^2 \\ &= (2A(t) + B(t)^2)\Sigma + (B(t)M + B_E(t)M + B_0(t))^2. \end{aligned}$$

This corresponds with the ODE for  $\Sigma$  in (3.3) and concludes the proof.  $\square$

## Appendix B. Proof of Lemma 5.3.

**B.1. Preparatory lemmas from [17].** Define the matrix  $M(\beta) \in \mathbb{R}^{(N+1) \times (N+1)}$  as

$$(B.1) \quad M(\beta) = \begin{bmatrix} 0 & \dots & \dots & 0 \\ 1 & 0 & \dots & 0 \\ \beta & 1 & 0 & \dots & 0 \\ \vdots & & \vdots & & \\ \beta^{N-1} & \beta^{N-2} & \dots & 1 & 0 \end{bmatrix}$$

LEMMA B.1 (Infinity norm of powers of  $M$ ). *The powers of the matrix  $M(\beta)$  have infinity norm*

$$(B.2) \quad \|M^k\|_\infty = \begin{cases} \min \left( \left( \frac{1-|\beta|^{N-1}}{1-|\beta|} \right)^k, \binom{N-1}{k} \right) & \text{if } |\beta| < 1 \\ |\beta|^{N-k-1} \binom{N-1}{k} & \text{else} \end{cases}$$

*Proof.* See [17, Lemma 4.3]  $\square$

LEMMA B.2 (Infinity norm of infinite-dimensional Toeplitz-operator  $M$ ). *In the case  $|\beta| < 1$ , it holds that the infinite-dimensional operator  $M(\beta)$  has infinity norm*

$$(B.3) \quad \|M(\beta)\|_\infty = \frac{1}{1-|\beta|}.$$

*Proof.* See [17, proof of Theorem 4.9]  $\square$

## B.2. Convergence with respect to iteration number of Parareal for scalar systems.

Boldfaced symbols are used to indicate vectors containing their non-boldfaced counterparts at all  $n = 0 \dots N$ , i.e.  $\mathbf{e}^k = [e_0^k \ e_1^k \ \dots \ e_N^k]^T$ .

LEMMA B.3 (Parareal error with affine propagators). *Denoting the effect of the scalar coarse propagator as  $\mathcal{C}(t, u) = Gu + g(t)$  and the fine propagator  $\mathcal{F}(t, u) = Fu + f(t)$ , the following recursion*



- [5] I. BOSSUYT, *Mc-moments*, 2023, <https://gitlab.kuleuven.be/u0124991/mMPareal.jl/-/tree/master/app/MC-moments>.
- [6] I. BOSSUYT, G. SAMAËY, AND S. VANDEWALLE, *Convergence of the Micro-Macro Parareal Method for a Linear Scale-Separated Ornstein-Uhlenbeck SDE*, submitted.
- [7] M. BOSSY, *Some stochastic particle methods for nonlinear parabolic PDEs*, ESAIM: Proceedings, 15 (2005), pp. 18–57, <https://doi.org/10.1051/proc:2005019>, <http://www.esaim-proc.org/10.1051/proc:2005019>.
- [8] M. BOSSY, J. FONTBONA, AND H. OLIVERO, *Synchronization of stochastic mean field networks of Hodgkin–Huxley neurons with noisy channels*, Journal of Mathematical Biology, 78 (2019), pp. 1771–1820, <https://doi.org/10.1007/s00285-019-01326-7>, <http://link.springer.com/10.1007/s00285-019-01326-7>.
- [9] M. BOSSY AND D. TALAY, *A stochastic particle method for the McKean-Vlasov and the Burgers equation*, Mathematics of Computation, 66 (1997), pp. 157–193, <https://doi.org/10.1090/S0025-5718-97-00776-X>, <http://www.ams.org/journal-getitem?pii=S0025-5718-97-00776-X>.
- [10] R. E. CAFLISCH, *Monte Carlo and quasi-Monte Carlo methods*, Acta Numerica, 7 (1998), pp. 1–49, <https://doi.org/10.1017/S0962492900002804>, [https://www.cambridge.org/core/product/identifier/S0962492900002804/type/journal\\_article](https://www.cambridge.org/core/product/identifier/S0962492900002804/type/journal_article).
- [11] J. DABAGHI, Y. MADAY, AND A. ZOIA, *A hybrid parareal Monte Carlo algorithm for parabolic problems*, Journal of Computational and Applied Mathematics, 420 (2023), p. 114800, <https://doi.org/10.1016/j.cam.2022.114800>, <https://linkinghub.elsevier.com/retrieve/pii/S0377042722004071>.
- [12] P. DEL MORAL AND J. TUGAUT, *On the stability and the uniform propagation of chaos properties of Ensemble Kalman–Bucy filters*, The Annals of Applied Probability, 28 (2018), <https://doi.org/10.1214/17-AAP1317>, <https://projecteuclid.org/journals/annals-of-applied-probability/volume-28/issue-2/On-the-stability-and-the-uniform-propagation-of-chaos-properties/10.1214/17-AAP1317.full>.
- [13] M. EMMETT AND M. L. MINION, *Toward an efficient parallel in time method for partial differential equations*, Communications in Applied Mathematics and Computational Science, 7 (2012), <https://doi.org/10.2140/camcos.2012.7.105>, <https://projecteuclid.org/euclid.camcos/1513732042>. ISBN: 0001404105.
- [14] S. ENGBLOM, *Parallel in Time Simulation of Multiscale Stochastic Chemical Kinetics*, Multiscale Modeling & Simulation, 8 (2009), pp. 46–68, <https://doi.org/10.1137/080733723>, <http://epubs.siam.org/doi/10.1137/080733723>.
- [15] R. D. FALGOUT, S. FRIEDHOFF, T. V. KOLEV, S. P. MACLACHAN, AND J. B. SCHRODER, *Parallel Time Integration with Multigrid*, SIAM Journal of Scientific Computing., 36 (2014), pp. C635–C661, <https://doi.org/10.1137/130944230>.
- [16] M. J. GANDER, *50 Years of Time Parallel Time Integration*, in Multiple Shooting and Time Domain Decomposition Methods, T. Carraro, M. Geiger, S. Körkel, and R. Rannacher, eds., vol. 9, Springer International Publishing, Cham, 2015, pp. 69–113, [https://doi.org/10.1007/978-3-319-23321-5\\_3](https://doi.org/10.1007/978-3-319-23321-5_3), [https://link.springer.com/10.1007/978-3-319-23321-5\\_3](https://link.springer.com/10.1007/978-3-319-23321-5_3). Series Title: Contributions in Mathematical and Computational Sciences.
- [17] M. J. GANDER AND S. VANDEWALLE, *Analysis of the parareal time-parallel time-integration method*, SIAM Journal on Scientific Computing, 29 (2007), pp. 556–578, <https://doi.org/10.1137/05064607X>, <https://epubs.siam.org/doi/abs/10.1137/05064607X>.
- [18] A.-L. HAJI-ALI AND R. TEMPONE, *Multilevel and Multi-index Monte Carlo methods for the McKean–Vlasov equation*, Statistics and Computing, 28 (2018), pp. 923–935, <https://doi.org/10.1007/s11222-017-9771-5>, <http://link.springer.com/10.1007/s11222-017-9771-5>.
- [19] D. J. HIGHAM AND P. E. KLOEDEN, *An introduction to the numerical simulation of stochastic differential equations*, no. 169 in Other titles in applied mathematics, Society for Industrial and Applied Mathematics, Philadelphia, 2021.
- [20] A. H. JAZWINSKI, *Stochastic processes and filtering theory*, no. v. 64 in Mathematics in science and engineering, Academic Press, New York, 1970.
- [21] P. KLOEDEN AND T. SHARDLOW, *Gauss-quadrature method for one-dimensional mean-field sdes*, SIAM Journal on Scientific Computing, 39 (2017), pp. A2784–A2807, <https://doi.org/10.1137/16M1095688>, <https://epubs.siam.org/doi/10.1137/16M1095688>.
- [22] P. E. KLOEDEN AND E. PLATEN, *Numerical solution of stochastic differential equations*, no. 23 in Applications of mathematics, Springer, Berlin ; New York, corr. 3rd print ed., 1999.
- [23] M. KOSTUR, J. LUCZKA, AND L. SCHIMANSKY-GEIER, *Nonequilibrium coupled Brownian phase oscillators*, Physical Review E, 65 (2002), p. 051115, <https://doi.org/10.1103/PhysRevE.65.051115>, <https://link.aps.org/doi/10.1103/PhysRevE.65.051115>.
- [24] F. LEGOLL, T. LELIÈVRE, K. MYERSCOUGH, AND G. SAMAËY, *Parareal computation of stochastic differential equations with time-scale separation: a numerical convergence study*, Computing and Visualization in Science, 23 (2020), <https://doi.org/10.1007/s00791-020-00329-y>, <https://doi.org/10.1007/s00791-020-00329-y>.

- s00791-020-00329-y.
- [25] F. LEGOLL, T. LELIEVRE, AND G. SAMAEY, *A micro-macro parareal algorithm: application to singularly perturbed differential equations*, SIAM journal on scientific computing, 2013-01, 35 (2013), pp. p.A1951–A1986.
  - [26] J.-L. LIONS, Y. MADAY, AND G. TURINICI, *Résolution d'edp par un schéma en temps "pararéel"*, Comptes Rendus de l'Académie des Sciences - Series I - Mathematics, 332 (2001), pp. 661–668, [https://doi.org/https://doi.org/10.1016/S0764-4442\(00\)01793-6](https://doi.org/https://doi.org/10.1016/S0764-4442(00)01793-6).
  - [27] M. L. MINION, *A hybrid parareal spectral deferred corrections method*, Communications in Applied Mathematics and Computational Science, 5 (2010), pp. 265–301, <https://doi.org/10.2140/camcos.2010.5.265>.
  - [28] E. NAJAFI, R. BABUŠKA, AND G. A. D. LOPES, *A fast sampling method for estimating the domain of attraction*, Nonlinear Dynamics, 86 (2016), pp. 823–834, <https://doi.org/10.1007/s11071-016-2926-7>, <http://link.springer.com/10.1007/s11071-016-2926-7>.
  - [29] M. NEUMÜLLER AND A. THALHAMMER, *Combining Space-Time Multigrid Techniques with Multilevel Monte Carlo Methods for SDEs*, in Domain Decomposition Methods in Science and Engineering XXIV, P. E. Bjørstad, S. C. Brenner, L. Halpern, H. H. Kim, R. Kornhuber, T. Rahman, and O. B. Widlund, eds., vol. 125, Springer International Publishing, Cham, 2018, pp. 493–501, [https://doi.org/10.1007/978-3-319-93873-8\\_47](https://doi.org/10.1007/978-3-319-93873-8_47), [http://link.springer.com/10.1007/978-3-319-93873-8\\_47](http://link.springer.com/10.1007/978-3-319-93873-8_47). Series Title: Lecture Notes in Computational Science and Engineering.
  - [30] M. NEUMÜLLER AND A. THALHAMMER, *A Fully Parallelizable Space-Time Multilevel Monte Carlo Method for Stochastic Differential Equations with Additive Noise*, SIAM Journal on Scientific Computing, 40 (2018), pp. C388–C400, <https://doi.org/10.1137/17M1146725>, <https://epubs.siam.org/doi/10.1137/17M1146725>.
  - [31] B. W. ONG AND J. B. SCHRODER, *Applications of time parallelization*, Computing and Visualization in Science, 23 (2020), p. 11, <https://doi.org/10.1007/s00791-020-00331-4>, <https://link.springer.com/10.1007/s00791-020-00331-4>.
  - [32] G. A. PAVLIOTIS, *Stochastic Processes and Applications: Diffusion Processes, the Fokker-Planck and Langevin Equations*, vol. 60 of Texts in Applied Mathematics, Springer New York, New York, NY, 2014, <https://doi.org/10.1007/978-1-4939-1323-7>, <https://link.springer.com/10.1007/978-1-4939-1323-7>.
  - [33] C. RACKAUCKAS AND Q. NIE, *DifferentialEquations.jl – A Performant and Feature-Rich Ecosystem for Solving Differential Equations in Julia*, Journal of Open Research Software, 5 (2017), p. 15, <https://doi.org/10.5334/jors.151>, <https://openresearchsoftware.metajnl.com/article/10.5334/jors.151/>.
  - [34] R. RODRIGUEZ AND H. C. TUCKWELL, *Statistical properties of stochastic nonlinear dynamical models of single spiking neurons and neural networks*, Physical Review E, 54 (1996), pp. 5585–5590, <https://doi.org/10.1103/PhysRevE.54.5585>.
  - [35] D. RUPRECHT, *Shared Memory Pipelined Parareal*, in Euro-Par 2017: Parallel Processing, F. F. Rivera, T. F. Pena, and J. C. Cabaleiro, eds., vol. 10417, Springer International Publishing, Cham, 2017, pp. 669–681, [https://doi.org/10.1007/978-3-319-64203-1\\_48](https://doi.org/10.1007/978-3-319-64203-1_48), [https://link.springer.com/10.1007/978-3-319-64203-1\\_48](https://link.springer.com/10.1007/978-3-319-64203-1_48). Series Title: Lecture Notes in Computer Science.
  - [36] D. SCHNOERR, G. SANGUINETTI, AND R. GRIMA, *Validity conditions for moment closure approximations in stochastic chemical kinetics*, The Journal of Chemical Physics, 141 (2014), p. 084103, <https://doi.org/10.1063/1.4892838>, <https://pubs.aip.org/aip/jcp/article/352569>.
  - [37] A. SUKYS AND R. GRIMA, *MomentClosure.jl: automated moment closure approximations in Julia*, Bioinformatics, 38 (2021), pp. 289–290, <https://doi.org/10.1093/bioinformatics/btab469>, <https://academic.oup.com/bioinformatics/article/38/1/289/6309452>.
  - [38] A.-S. SZNITMAN, *Topics in propagation of chaos*, in Ecole d'Été de Probabilités de Saint-Flour XIX — 1989, P.-L. Hennequin, ed., vol. 1464, Springer Berlin Heidelberg, Berlin, Heidelberg, 1991, pp. 165–251, <https://doi.org/10.1007/BFb0085169>, <http://link.springer.com/10.1007/BFb0085169>. Series Title: Lecture Notes in Mathematics.
  - [39] Y. TANG, R. YUAN, G. WANG, X. ZHU, AND P. AO, *Potential landscape of high dimensional nonlinear stochastic dynamics with large noise*, Scientific Reports, 7 (2017), p. 15762, <https://doi.org/10.1038/s41598-017-15889-2>, <http://www.nature.com/articles/s41598-017-15889-2>.
  - [40] A. THALHAMMER, *Numerical methods for stochastic partial differential equations: Analysis of stability and efficiency*, PhD thesis, Johannes Kepler Universität Linz, 2017.
  - [41] C. VILLANI, *Optimal transport: old and new*, no. 338 in Grundlehren der mathematischen Wissenschaften, Springer, Berlin, 2009.
  - [42] N. ZAGLI, G. A. PAVLIOTIS, V. LUCARINI, AND A. ALECIO, *Dimension reduction of noisy interacting systems*, Physical Review Research, 5 (2023), p. 013078, <https://doi.org/10.1103/PhysRevResearch.5.013078>, <https://link.aps.org/doi/10.1103/PhysRevResearch.5.013078>.
  - [43] S. ZHANG, D. WIDMANN, AND D. S. BARREIRA, *Juliaoptimaltransport/optimaltransport.jl: v0.3.19*, Jan. 2022, <https://doi.org/10.5281/zenodo.5920148>, <https://doi.org/10.5281/zenodo.5920148>.